Limnol. Oceanogr., 55(1), 2010, 279–288

Temporal and spatial features of the thermohydrodynamics of shallow salty lagoons in northern Chile

Alberto de la Fuente*,[1] and Yarko Niño

Departamento de Ingeniería Civil, Universidad de Chile, Santiago, Chile

Abstract

Salares in the altiplanic region of Chile, Bolivia, and Argentina sustain important ecosystems in small, shallow wetlands, with inflows provided by groundwater and outflows consisting mainly of evaporation. The temporal and spatial thermohydrodynamics of one of these extremely shallow, saline, endorheic wetlands in northern Chile is analyzed on the basis of field observations of water temperature and salinity, and low-dimensionality models accounting for conservation of heat, mass, and volume. Temperature in the studied system is spatially homogeneous but with strong daily oscillations. Salinity, on the other hand, exhibits longitudinal gradients from the zone of (salty) groundwater upwelling to the final evaporation lagoon. Heat balance in the system is largely controlled by wind, as the evaporative heat flux balances out the net solar radiation. Heat exchange with the bottom sediments damps the daily temperature oscillations by retaining (releasing) heat from (to) the water column. Simulated longitudinal profiles of salinity and flow discharge agree reasonably well with field observations but salinity effects on the rates of both evaporation and salt precipitation need to be taken into account. Laboratory experiments were conducted to develop a simple model for the former effect while the latter effect was accounted for by using existing information. Field measurements provided calibration of the model parameters. The observed longitudinal salinity gradients are correlated with the biological structure of the associated ecosystem to explain, for instance, the existence of specific flamingos' feeding areas in the system.

Salares are landscapes formed by a crust of salt resulting from evaporation of water in saline lakes, which are typically located in central depressions of closed basins of the elevated plateau (with elevations of about 4000 m above sea level [asl]) of the Central Andes of Chile, Bolivia, and Argentina. This elevated plateau, locally known as Altiplano (which in Spanish means high and flat lands), is covered by numerous volcanoes and elevated mountains (with elevations up to about 6500 m asl) that delineate the closed basins (Risacher et al. 2003). Salar is a particular name for playas (Kampf et al. 2005), defined by Rosen (1994) as landscapes with negative annual water balance and a capillary fringe that is close enough to the surface as to allow for water discharge via evaporation.

Latitudes around the Tropic of Capricorn impose an arid climate characterized by low precipitation and air humidity (less than about 150 mm yr^{-1} and 50%, respectively) that explain potential evaporation rates greater than about 1000 mm yr^{-1} (Risacher et al. 2003). Furthermore, high altitude imposes low air temperature (of around 0°C annual mean), high solar radiation (up to about 1300 W m^{-2} in summer), and high daily and seasonal temperature oscillation with amplitudes that reach values greater than 30°C.

Aquatic ecosystems in salares are found as small and extremely shallow wetlands a few centimeters deep, sustained by inflows coming from groundwater that upwells at the perimeter of the salar (Risacher et al. 2003; Kampf et al. 2005; Houston 2007). Once the groundwater upwells, it is completely evaporated in an area defined by the balance between the inflow volume and evaporation rates. This balance thus produces the evapoconcentration of salt, increasing then the water salinity along the flow direction. These systems are known as VCL (D. Soto pers. comm.) because their structure can be decomposed into a marshland, or vega in Spanish (V), supplied by groundwater; a rather shallow channel flow (C), a few kilometers long; and an evaporation and infiltration lagoon (L) as it is shown in Fig. 1. Terrestrial vegetation is present only in the vegas, whereas the surrounding area of channels and lagoons is covered by a crust of salt.

These VCLs spread out in the desert, sustaining rich terrestrial (Rundel et al. 2003) and aquatic ecosystems (Hulbert and Keith 1979; Zuñiga et al. 1991), which have been focus of different biochemical (Messerli et al. 1997; Risacher et al. 2003; Kampf et al. 2005) and hydrological studies (Williams et al. 1995; Jerez 2000; Demergasso et al. 2003). Particular attention has been given to altiplanic flamingos, represented by three species: *Phoenicopterus chilensis*, *Phoenicopterus andinus*, and *Phoenicopterus jamesi*, with populations that reach thousands of birds per salar (Hulbert and Keith 1979). Two important aspects of the flamingos' behavior have been related with the physical dynamics of VCLs. First, these birds build their nests within the lagoons to protect them from the attack of predators such as the fox (Hulbert and Keith 1979); therefore, water has to be deep enough to provide real nest protection, but not as much to avoid flooding. Second, flamingos feed on benthic organisms only in particular areas of the VCLs. This specificity of feeding behavior has been explained on the basis of size selectivity, on the basis of the bill morphology, where the latter acts as a bandwidth filter (Hulbert and Chang 1983; Mascitti and Kravetz

* Corresponding author: aldelafu@ing.uchile.cl

[1] Present address: Centre for Water Research, The University of Western Australia

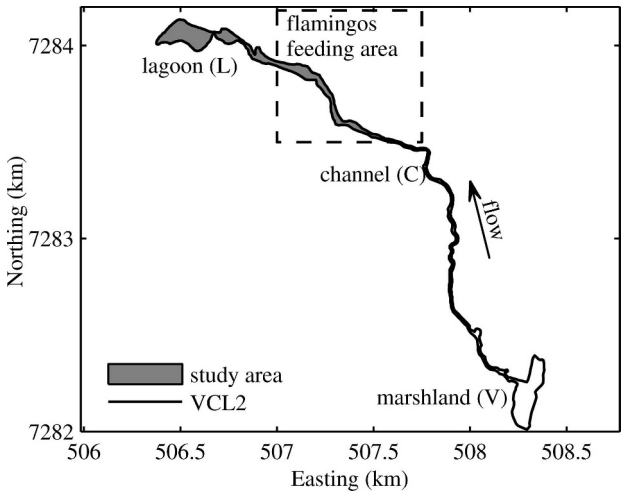

Fig. 1. Morphological decomposition of VCL2 and definition of study area.

2002). The existence of a relationship between flow regime, which controls water salinity and mass exchange between water and sediments, and the benthic dynamics that determines the availability of the specific type of food that constitutes the flamingos' diet is a plausible hypothesis to be tested to explain this observation.

Although the relationship between salinity and benthic organisms has been described for similar ecosystems (Campbell 1995; Ryves et al. 2006), no previous scientific studies on the hydrodynamics of altiplanic lagoons have been found, which is a major obstacle to accomplish the test of the above hypothesis. Different studies have described mass, energy, and salt balances for similar systems around the world, governed by evaporation (Helczeg and Imboden 1988; del Castillo and Farfán 1997; Birchoff et al. 2004); however, spatial changes driven also by diurnal oscillation of the meteorological conditions have not yet been included in previous analyses. The main objective of the study reported here was to define, on the basis of field data and mass, volume, and energy conservations laws, the main processes that modulate the thermohydrodynamics of one of these VCL systems, the focus being placed on characterizing and predicting the temporal and spatial changes in the water temperature and salinity. It is worth noting that aquatic ecosystems whose hydrology is determined by a balance between inflow and evaporation, which give rise to salty small-size lagoons, can also be found in other places where the results presented here can be applied (Williams 2002; Timms 2005; Costelloe et al. 2009).

With this aim, the system denoted VCL2 at Salar Punta Negra was chosen because it has a clear longitudinal structure, enabling us to propose a simplified analysis to identify the main processes involved in the thermohydrodynamics of these ecosystems. System VCL2 is located in northern Chile, about 200 km to the southeast of the city of Antofagasta and about 1500 km to the north of Santiago. The average water inflow to VCL2 is about 3.5 L s^{-1}, and this aquatic system is used by populations of flamingo for feeding. VCL2 is about 2.5 km long with a clear VCL subdivision (*see* Fig. 1): a marshland of about 300 × 100 m, a channel 1.5 km long and 10 m wide, and a transition zone where the flow width increases gradually to reach about 150 m at the lagoon.

This article is organized as follows: in section 2 the field measurements are described and discussed preliminarily, whereas in sections 3 and 4 the thermodynamics and mass and volume balances of the system are studied, respectively. Different conceptual models are proposed in section 5 to explain the spatial distribution of salinity and the results are compared against field measurements. A dimensional analysis is conducted in section 6 to propose an algebraic expression for the estimation of surface area and water salinity in VCL systems on the basis of characteristic inflow and evaporation rates. Finally, in section 7, the discussion is focused on proposing a general conceptual framework to describe the thermohydrodynamics of aquatic systems in salares, particularly the processes that control their spatial distribution of salinity, and its connection with the ecosystem dynamics.

Methods

Field study—Different field studies, previously reported by de la Fuente et al. (2006), were conducted covering the area delimited in Fig. 1. This area was chosen because it represents the flamingos' feeding zone and it is where the stronger salinity gradients are found. Within this area, a 2-d long field campaign was conducted between 11 and 13 January 2006, aimed at characterizing the hydrodynamics of VCL2. Measurements of salinity were taken with a portable WTW conductivimeter and thermometer to obtain three sets of measurements of the conductivity and temperature field in the study area, characterizing the morning, noon, and evening dynamics of the system. Measured data of electric conductivity and water temperature are internally converted by the instrument into salt concentration and this internal conversion was validated in the laboratory, for the range of salinities measured, with a solution of NaCl. Water inflow was of about 2.1 L s^{-1}, the flow being generally so shallow (1 to 5 cm deep) that the measurements taken at a point can be considered to be equivalent to vertical averages. The two-dimensional salinity field corresponding to measurements taken between 12:00 h and 13:00 h 12 January is plotted in Fig. 2A, whereas representative longitudinal profiles for the three sets of measurements taken during morning, noon, and evening, respectively, are shown in Fig. 2B. Each one of the three spatial characterizations of the water salinity was carried out through intensive sampling, in the whole domain, of water conductivity and temperature, recording also the global positioning system location of the measurement point. For each characterization, about 100 localized measurements were taken covering the whole domain and the postprocessing of the information was conducted using the contour function of Matlab. Furthermore, Fig. 2B shows some diurnal variation in the water salinity, with amplitude of about 40 g L^{-1}, such that the salinity increases during the afternoon because of diurnal variations in the evaporation rate, and then decreases during the night. These temporal changes in water salinity are more

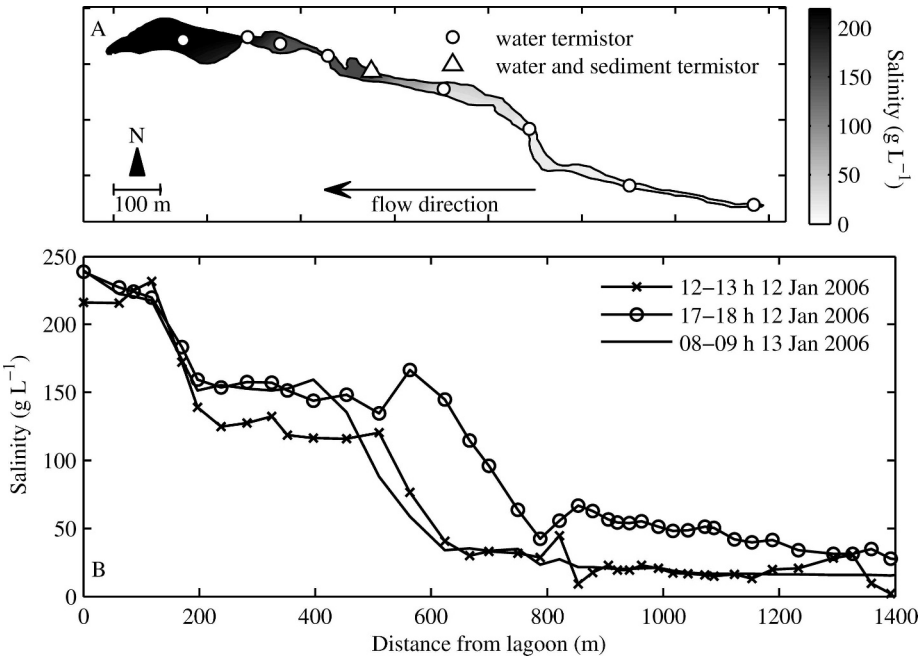

Fig. 2. (A) Contour plot for water salinity measurements at noon on 12 January 2006. Circles and triangle indicate locations where water and sediment temperature measurements were made. (B) Longitudinal profiles of salinity at three different times.

likely to occur in mid-regions of the channel, where the horizontal gradients in water salinity are larger.

Meteorological variables corresponding to air temperature, relative humidity, air pressure, net incident short-wave solar radiation, and wind speed and direction are available every 15 min from January to March of 2006. These measurements are shown as time series in Fig. 3 for the duration of the field campaign. The strongest wind speed occurs during the day and comes from the west, going from the lagoon to the marshland. During the night, the wind inverts its direction, coming from the marshland to the lagoon.

Nine Stowaway Tidbit thermistors were placed along VCL2 for measuring the spatial variation of water temperature and an additional one was placed 2 cm below the water–sediment interface at the points indicated in Fig. 2A. These measurements show that temperature tends to vary in time but not in space. Indeed, Fig. 4A shows time series of the spatially averaged value of water temperature (measured by the first nine thermistors) and maximum and minimum values of these measurements for each time. Variation in space does not exhibit a trend and is much smaller than that observed in time (Fig. 4A). On the other hand, Fig. 4B shows the measured temperature of the bottom sediments, which displays similar diurnal oscillations as those of the water column. This issue is discussed hereafter.

The low inflows characteristic of the hydrodynamic conditions of VCL2 produce water depths between 1 and 5 cm, and flow velocities lower than 10 cm s^{-1}; both ranges were measured during field studies. Thus, flow conditions correspond to Reynolds number values (on the basis of water depth and mean flow velocity) of about 1500, close to the laminar flow limits.

Results

Thermodynamic balance—Given the spatial homogeneity of the temperature in the system, it is assumed that it can be modeled using a spatially averaged equation that accounts only for temperature variations in time. Heat balance in a water volume of depth h, density ρ, heat capacity c_p, and temperature T_w is described by (Garratt, 1992; Bogan et al. 2003)

$$(\rho c_p) h \frac{\partial T_w}{\partial t} = H_{SW}^{\downarrow} - H_{SW}^{\uparrow} + H_{LW}^{\downarrow} - H_{LW}^{\uparrow} + H_S + H_L + H_G \quad (1)$$

Subindexes denote the nature of the corresponding flux: short-wave radiation (SW), long-wave radiation (LW), sensible or convective heat flux (S), latent or evaporative heat flux (L), and heat exchange with the bottom sediment (G). Arrow denotes fluxes to ($\downarrow$) or from ($\uparrow$) the water. $H_{SW}^{\downarrow}$ was measured in the system (Fig. 3E) and the fraction refracted at the water surface was estimated on the basis of the albedo, assumed equal to 3%. Long-wave radiation was computed using the Stefan–Boltzman relationship,

$$H_{LW}^{b} = \varepsilon \sigma T_{AW}^{4} \quad (2)$$

where ε is the emissivity of the medium, taken equal to 0.97, which is a characteristic value for water and clear sky; $\sigma = 4.899 \times 10^{6}$ kJ m^{-2} d^{-1} °K^{-4} and T_{AW} takes values of the air or water temperature in Kelvin degrees, depending on whether water or atmospheric emissions are computed

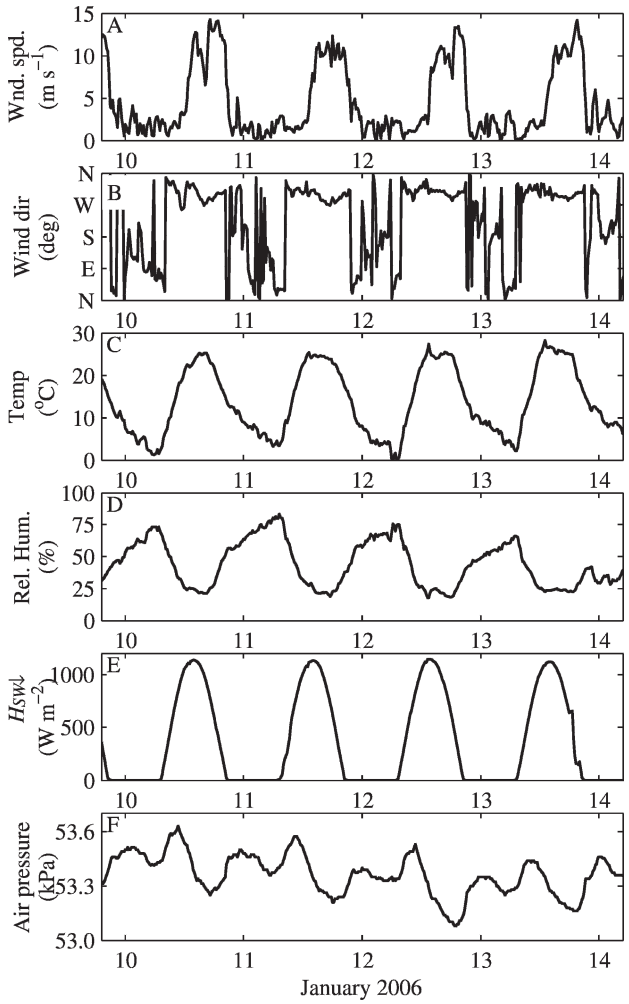

Fig. 3. Time series of meteorological data. (A) Wind speed, (B) wind direction, (C) air temperature, (D) relative humidity, (E) incident short-wave radiation, and (F) air pressure. Source: de la Fuente et al. (2006).

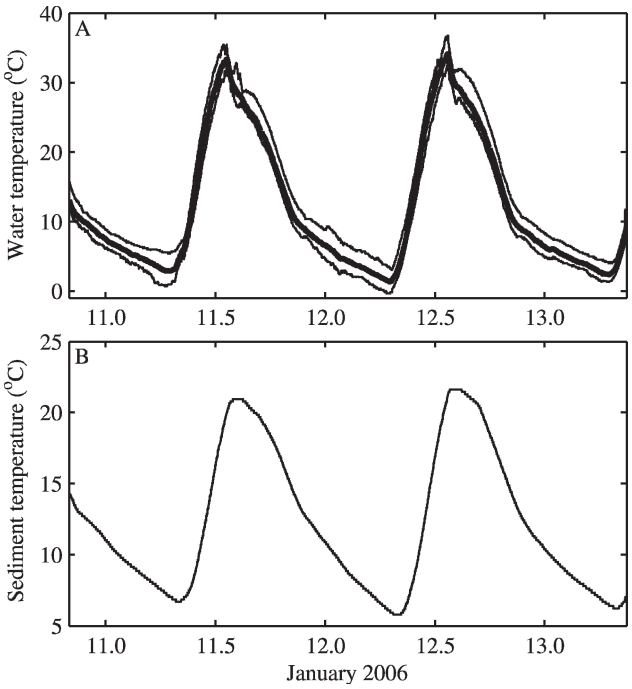

Fig. 4. Temperature of the (A) water column (spatial mean, maximum, and minimum values) and (B) sediment bed (taken at 2 cm below the sediment–water interface).

(Figs. 5A and 3C, respectively). To compute the sensible and latent heat fluxes, both atmospheric turbulence and stability were considered (Mahrt and Ek 1984; Adams et al. 1990). For that, the Monin–Obukhov similarity theory for nonneutral surface layer was applied, with the parameterizations of the Kansas experiments (Garratt 1992). Finally, the hydrodynamic roughness was computed with the expression proposed by Gulliver and Song (1986) for smooth surface, capillary wave, and gravitational wave regimes. Figure 5 shows the atmospheric heat fluxes computed on the basis of the field data. Dark and light lines in Fig. 5 were computed using the spatial mean, minimum, and maximum thermistor water temperature, as in Fig. 3A.

The net sensible heat balance within a day is close to zero, with maximum and minimum values less than about 10% of the net solar radiation (Fig. 5C); therefore, this term is not very important in the heat balance. On the other hand, long-wave radiation (Fig. 5B) extracts heat from the water all day long, with a maximum rate that correlates in time with the water temperature maximum. The net solar radiation (Fig. 5A) is mainly balanced by the evaporative heat flux (Fig. 5D), which, although it increases in magnitude as the temperature increases, is mainly driven by the wind blowing during the afternoon, which, in turn, increases the rate of water diffusion to the atmosphere, reaching maximum evaporation rates of about 40 mm d^{-1} and a mean daily value of about 8 mm d^{-1} (Fig. 5E). One extra computation was carried out, as a sensitivity analysis for the evaporative heat flux, not accounting for the atmospheric boundary layer (ABL) stability. The difference between evaporation rates with and without considering ABL stability is shown in Fig. 5F, where a positive value means that the evaporation rate computed by considering the ABL stability is larger than if it is not considered. The maximum difference between computed evaporation rates is about 2 mm d^{-1}, which is equivalent to about 50 W m^{-2} in terms of heat flux, and this maximum is detected before the wind starts blowing at about noon (Fig. 3A). This change in behavior due to wind blowing shows that during the morning, the buoyancy vertical fluxes are important to explain heat exchange between the VCL2 and the atmosphere, while in the afternoon, it is turbulence in the ABL, produced by wind shear, that controls such heat exchange. Figure 5F also shows that the thermodynamics balance given here for VCL2 is not dependent on the parameterization assumed for the turbulent conditions in the ABL.

When the net atmospheric flux is computed and compared with the left hand side of Eq. 1 (Fig. 6B), the heat exchange with the bottom sediments clearly closes the balance. This exchange releases heat during the night (light

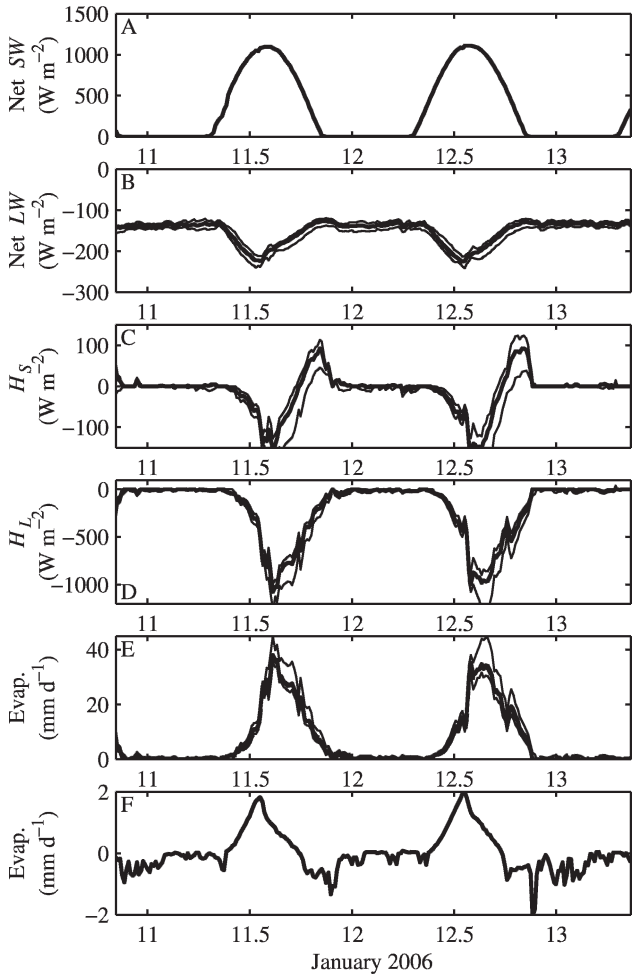

Fig. 5. Atmospheric heat fluxes in W m^{-2}: (A) net short-wave radiation, (B) net long-wave radiation, (C) sensible flux, and (D) latent heat flux. (E) Potential evaporation rates computed considering the atmospheric boundary layer (ABL) stability, and (F) difference between evaporation rate computed with and without considering the ABL stability.

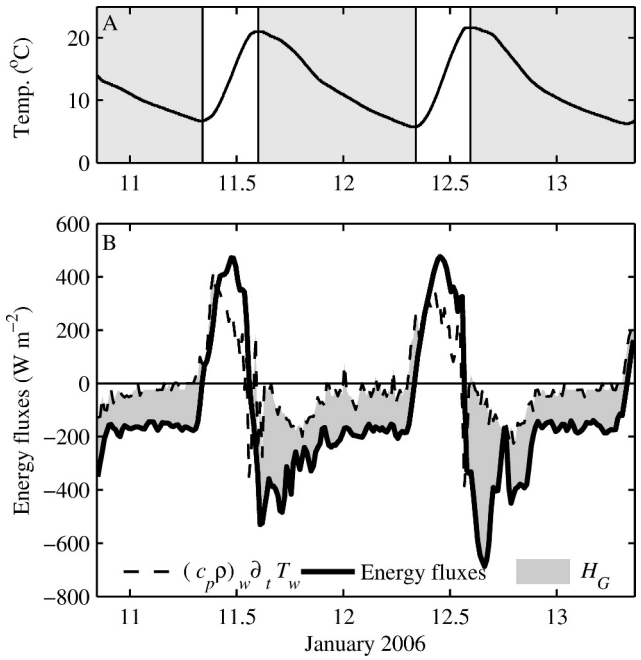

Fig. 6. Dynamics of ground heat flux: (A) time series of sediment temperature measurements; gray area shows flux from water to sediment. (B) Comparison between net atmospheric fluxes and term $\rho c_p h \partial_t T$; gray areas denote when ground heat flux is positive from sediment to water column.

gray filled areas in Fig. 6), which balances out the long-wave emission, maintaining water temperature higher than it would be without this flux. On the other hand, during the morning when the water temperature begins to increase, sediments capture a part of this heat, producing the opposite effect than during the night. This heat exchange at the sediment–water interface clearly explains the high daily oscillation of sediment temperature observed in the system (Fig. 4B).

Mass and volume balances—The hydrological regime of VCL2 is characterized, as a first approximation, by an average inflow of about 3.5 L s^{-1} and the hydrological balance is closed by considering evaporation losses, which reach a daily average value up to 14 mm d^{-1} in January (austral summer), with a mean value of about 8 mm d^{-1} during the field campaign. These high evaporation rates produce the spatial differences of salinity along the flow direction, which is minimum nearly at the marshland, with a constant concentration of about 15 g L^{-1} (note that the groundwater is saline in this region and this inflow concentration varies in less than about 5% over time), and increases downstream due to the evapoconcentration of salt ions produced by the reduction of the dilution volume due to evaporation.

It is worth noting that this conceptual description neglects at least two mechanisms that may influence mass and volume balances in the VCL: dissolution of previously deposited salts and infiltration. Although the dissolution of previously deposited salts along the channel could also explain the observed positive longitudinal salinity gradients along the VCL, it is argued that this process would be important only in the long term as it would impose morphological changes in the channel, which to our knowledge have not been seen or reported. On the contrary, changes in the lagoon morphology, associated with local salt precipitation, can be detected even within one season. Possible water and salt exchanges between the VCL and the confined salty aquifer that lies below the land surface (Risacher et al. 2003), on the other hand, should be considered as a source of fresher water for the surface system, because the groundwater piezometric level of the confined aquifer is generally above the land surface level, which explains the water upwelling at the upstream end of the VCL. Therefore, in case important water exchanges between the VCL and the aquifer occur, they would decrease the surface water salinity and contribute to lowering the longitudinal salinity gradients along the system, because the groundwater salinity is not being evapoconcentrated as in the VCL2.

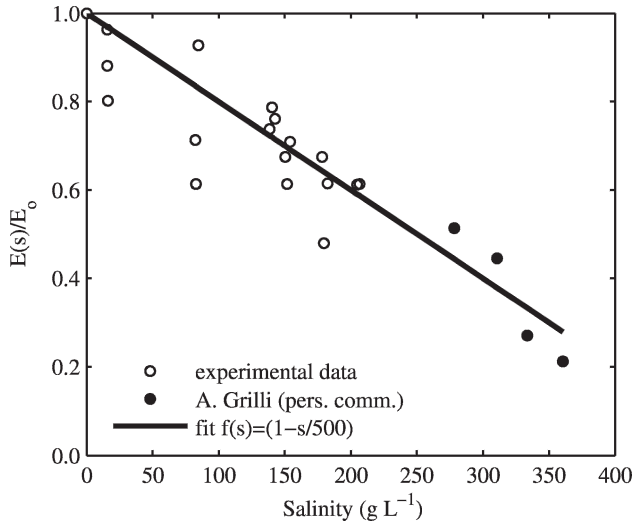

Fig. 7. Empirical relationship between water salinity and correction for evaporation. Present laboratory data (clear symbols) and field data of A. Grilli (pers. comm.) (solid symbols).

Regarding the volume conservation in the entire system, the inverse relationship between the net evaporation rate and water salinity (Oround 1999; Lensky et al. 2005) should be included in the computation of the actual evaporation rates from VCL2. According to Oround (1999) and Lensky et al. (2005), this inverse relationship decreases the water saturation in the air because of reductions in the free energy of water molecules. To take into account this process, the parameter β is introduced such that the evaporated mass E kg m^{-2} s^{-1} is computed as

$$E(S) = K\,\rho_a(\beta q_s - q) \tag{3}$$

where K is the bulk transfer coefficient computed with the Monin–Obukhov theory, ρ_a the air density, and q_s and q the water concentration, saturated and in the air, respectively (Garratt 1992). A value of β equal to 1 corresponds to pure water, which yields the so-called potential evaporation.

However, Grilli (pers. comm.) used a simple approach on the basis of field data from other Andean salt lagoons, such that the effect of water salinity on the evaporation rate is taken into account by means of a function $F(S) = E(S)/E_o$, where E_o is the potential evaporation rate given by $\beta = 1$ in Eq. 3, using field data of very high salinity (about 350 g L^{-1}, see Fig. 7). To validate Grilli's analysis and to extend the proposed trend toward lower salinity values, laboratory experiments were conducted as part of the present study. For these experiences, water of different salinity, including the case with no salinity, prepared by mixing distilled water and salt (NaCl) in different proportions, was evaporated simultaneously from a set of ponds under controlled conditions of ambient temperature and humidity. The evaporation rate was computed by measuring differences in mass with respect to the initial condition for each pond. The results obtained in these simple experiments agree fairly well with field data at high salinity, and suggest a linear reduction of the evaporation rate as salinity increases (Fig. 7).

Considering a characteristic potential evaporation rate of 8 mm d^{-1}, and the experimental correction of the evaporation acting together with the spatial distribution of salinity of Fig. 2A, the total evaporated water volume from VCL2 is estimated in 3.7 L s^{-1}. Were the relationship of Fig. 7 not considered, the evaporated water flow would be equal to 6 L s^{-1}, which is about two times greater than the mean inflow rate.

With regard to salt mass balance within VCL2, as has been mentioned, the salt concentration in the marshland is about 15 g L^{-1} with variations of less than about 5%. This concentration and the mean inflow rate give a mean input of salt mass into the VCL system equal to about 4500 kg d^{-1}, equivalent to 2.1 m^3 d^{-1} of salt that is precipitated in the lagoon, thus increasing its bed elevation and changing its morphology. It can be argued that precipitation occurs mainly in the lagoon, because during the field campaign it was easy to appreciate that the bed composition in this area is actually a crust of salt, whereas the bed composition in other areas of the system is basically clay and silt and a mat of organic matter.

Measurements plotted in Fig. 2 show an almost constant salinity in the entire lagoon, with maximum values of about 230 g L^{-1}. Such value is about half that of the maximum salinity that according to Fig. 7 reduces the evaporation rate to zero, which is about 500 g L^{-1}. This result points out that a saturation mechanism maintains the evaporation rate in the lagoon at levels lower than those predicted by Fig. 7. It is argued that this mechanism corresponds to salt precipitation. Indeed, salinity data corresponding to saturation concentration (Benduhn and Renard 2004) reach values that agree fairly well with those of the maximum salinity measured in VCL2. It is, therefore, important to consider the process of salt precipitation to close the water balance. If that is the case, it should be noted that the saturation threshold should be dependent on water temperature and type of ions defining the salinity solution; however, Na^+ and Cl^- ions are the most dominant in altiplanic water (Risacher et al. 2003) and the limit of 500 g L^{-1} can then be used as a representative value for VCL systems in the altiplano, although this value should be interpreted as a daily average value for summer conditions.

Spatial dynamics—The evapoconcentration problem can be described using mass and volume conservation equations for a one-dimensional steady flow in a channel of width B m, with water and salinity inflows at the upstream boundary, Q_o m^3 s^{-1} and S_o g L^{-1}, respectively. This problem is analyzed under three different approaches.

Case 1: Case in which longitudinal changes in the water flow Q are given by a homogeneous potential evaporation rate E_o, and changes in the water salinity respond to the fact that the dilution volume decreases because of the water evaporation, the total mass being preserved in the system. This dynamic gives the governing equations for

conservation of volume and salinity along the longitudinal axis

$$\frac{\partial Q}{\partial x} = -E_o\ B$$
$$Q\frac{\partial S}{\partial x} - E_o\ B\ S = 0 \tag{4}$$

Case 2: This case considers that the net evaporation is now corrected for salinity effect, such that the correction is described by a linear function that takes a value equal to 1 for $S = 0$ and 0 for $S = S_m$ (Fig. 7), where S_m is the maximum salinity. The salt balance is described by the same dynamics as in case 1, and the governing equations are

$$\frac{\partial Q}{\partial x} = -E_o\ B\left(1 - \frac{S}{S_m}\right)$$
$$Q\ \frac{\partial S}{\partial x} - E_o\ B\ S\left(1 - \frac{S}{S_m}\right) = 0 \tag{5}$$

Case 3: This case considers that the evaporation is corrected for salinity effect as for case 2, but the salt is allowed to precipitate when its concentration exceeds a saturation concentration S_p. The precipitation rate is assumed to be constant, characterized by a precipitation velocity kp m s^{-1}. The governing equations are now written as

$$\frac{\partial Q}{\partial x} = -E_o\ B\left(1 - \frac{S}{S_m}\right)$$
$$Q\ \frac{\partial S}{\partial x} - E_o\ B\ S\left(1 - \frac{S}{S_m}\right) = -B\ \max\left(kp\ \left[S - S_p\right], 0\right) \tag{6}$$

S_m is the maximum salinity that produces evaporation, which was determined to be equal to 500 g L^{-1} on the basis of field measurements and laboratory experiments (Fig. 7). S_p is the saturation salinity, estimated as 200 g L^{-1} on the basis of data by Benduhn and Renard (2004). Finally, kp is the bulk precipitation coefficient that should be a function of flow regime and water temperature; however, as no previous studies were found on this issue, the value of this coefficient was estimated by fitting the model to the present field measurements. Notice that the threshold concentration S_p is also dependent on water temperature, and thus changes during the day. Particularly, the precipitation limit increases with the temperature (Benduhn and Renard 2004), the salt precipitation being a process that is more likely to occur during the night when the water temperature decreases and wind mixing of the systems recedes. However, given the steady state analyzed here, this given value for S_p should be considered as representative of the daily average conditions during summer, and may change during the year.

Figure 8A shows the longitudinal salinity profile measured in the afternoon of 13 January, and those predicted under the three approaches previously explained for E_o = 8 mm d^{-1}, corresponding to the mean daily evaporation estimated in Fig. 5E, an estimated value of kp = 40 mm d^{-1} and the measured data Q_o = 2.1 L s^{-1}, S_o = 25 g L^{-1}, and B = 25 m. Figure 8B shows the longitudinal profiles of water flow discharge computed with the three proposed

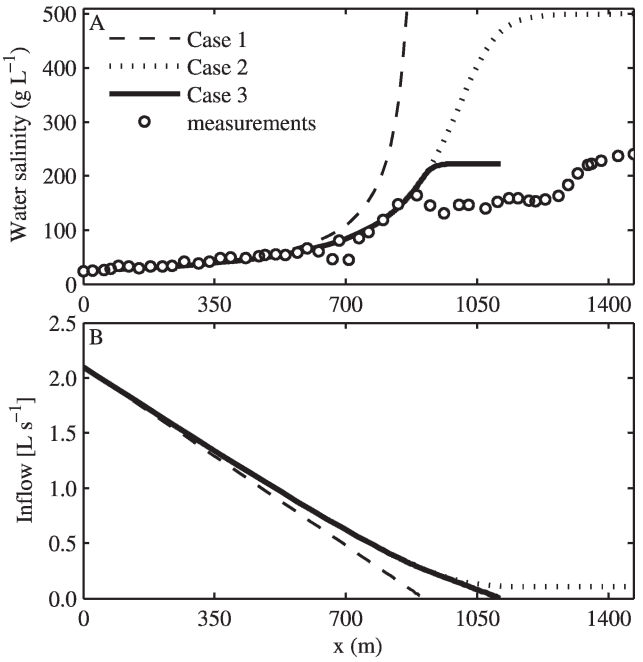

Fig. 8. Results of the simulations given by different conceptual models for salt and mass balance in a 1D evapoconcentrated channel. Longitudinal profiles of (A) salinity and (B) water flow rate.

approaches. Dashed line in Fig. 8 corresponds to the longitudinal profiles under the first approach with constant evaporation. Such assumption gives a faster increase of salinity along x than was measured, and an infinite concentration of salt at a distance $x_* = Q_o/(E_oB)$, where also $Q = 0$. Under the second approach (solid light line in Fig. 8) the longitudinal salinity profile fits well the field measurements, and reaches a finite salinity at a distance greater than x_*; however, as the evaporation is cut off at a salinity of 500 g L^{-1}, the water flow is not completely evaporated in the system, giving an infinite VCL longitude.

Finally, when salt precipitation is switched on (third approach, solid dark line in Fig. 8), the good fit of the modeled longitudinal salinity profile to the field data obtained for $S < S_p$ under the second approach is still present. Beyond the point where the salinity reaches the limit value $S = S_p$, this variable remains constant around this value, and therefore evaporation can account for all the inflow volume within a finite distance. Despite these generally positive results, fit of the computed longitudinal profile to measurements is not perfect. Particularly, the computed distance required to completely evaporate the water inflow in VCL2 is shorter than observed in the field, which leads to underestimation of the total length of the system. Nevertheless, taking into account that the present analysis neglects the longitudinal variation of the width B and that steady flow was assumed for the analysis, it is concluded that this simple conceptual scheme can explain the main features of the salinity dynamics in the VCL system under study.

Dimensional analysis and generalization of the results—Previous sections have allowed us to identify the mechanisms, evaporation and salt precipitation, that primarily

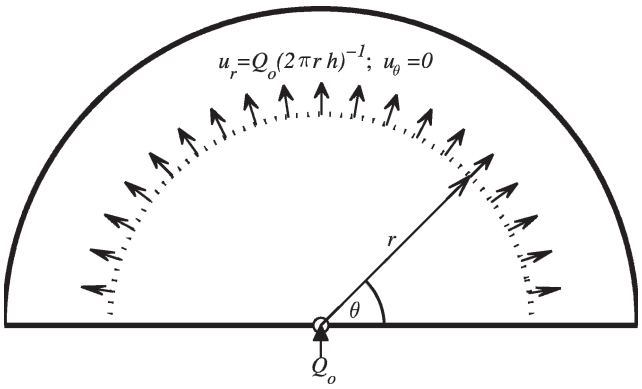

Fig. 9. Conceptual scheme for the 2D radial problem in semicircular domain.

explain the spatial distribution of salinity in altiplanic lagoons. Even though the results obtained in the previous section can be readily extended to other systems where channel-type morphology could be assumed, it is worth noting that, at least in the Chilean altiplano, there are only few cases where that assumption is not questionable. In fact, cases where the inflow water does not canalize are more frequent in the altiplanic region, which can be represented by a semicircular domain (Fig. 9), where volume and salt mass governing equations are written in polar coordinates as

$$\frac{\partial Q}{\partial r} = -\pi\, r\, E_o \left(1 - \frac{S}{S_m}\right)$$
$$Q\,\frac{\partial S}{\partial r} - \pi\, r\, E_o\, S \left(1 - \frac{S}{S_m}\right) = -\pi\, r \max\left(kp\,\left[S - S_p\right], 0\right) \tag{7}$$

On the basis of both types of morphology, channel and semicircular domain, a dimensional analysis is conducted, as follows, to analyze the dependence of the solution (S and Q) on the parameters that define the problem, which are E_o, S_m, S_p, kp, and Q_o. In particular, we would like to predict the size or horizontal extension of the VCL system, given a set of control parameters. The accumulated surface area (Ω) is used instead of the horizontal dimensions of the problem (x or r for the channel and semicircular domains, respectively), where this is defined as the VCL surface area between 0 and x or r, Ω_o being the maximum VCL surface area where also $Q = 0$.

Four dimensionless parameters define the behavior of Ω_o: $\Pi_1 = E_o \Omega_o Q_o^{-1}$, $\Pi_2 = S_p S_m^{-1}$, $\Pi_3 = S_o S_m^{-1}$, and $\Pi_4 = kp E_o^{-1}$. Figure 10A shows the plot of Π_1 as a function of Π_4 (for constant values of $\Pi_2 = 0.4$ and $\Pi_3 = 0.03$ given by the values of $S_o = 15$ g L^{-1}, and S_p and S_m estimated in previous sections for VCL2) using the solution of the one-dimensional (1D) (channel-like morphology, Eq. 6) and two-dimensional (2D) (semicircular morphology, Eq. 7) cases, both solutions being identical. For small values of kp (small Π_4) the solution tends to that without precipitation; therefore, the maximum salinity goes to S_m and the surface area to infinite. On the contrary, greater values of kp (large Π_4) produce faster salt precipitation with maximum salinity closer to S_p, and there is a certain value for this parameter above which the solution does not depend on it. This behavior and the established limit of $S_p \approx 200$ g L^{-1} suggest

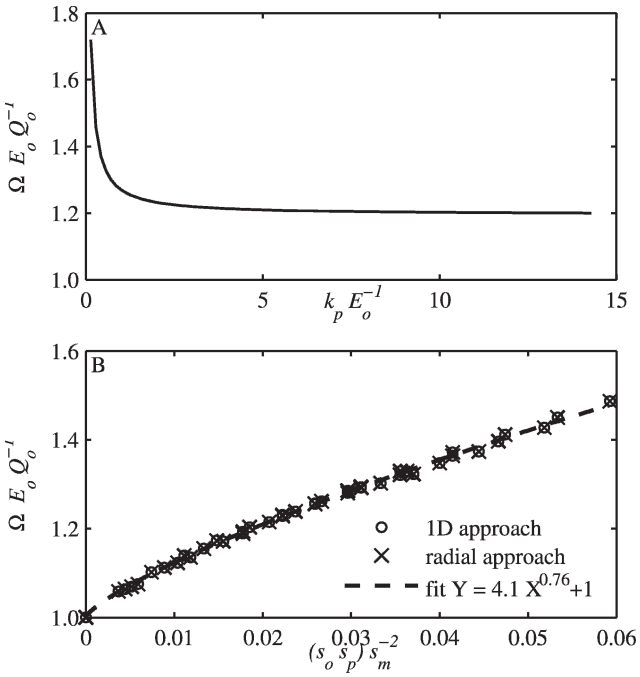

Fig. 10. Dimensionless VCL surface $\Pi_1 = \Omega E_o Q_o^{-1}$ as a function of (A) dimensionless number $\Pi_4 = k_P E_o^{-1}$ for constant values of $\Pi_2 = 0.4$ and $\Pi_3 = 0.03$, and (B) the product $\Pi_2\Pi_3 = S_o S_p S_m^{-2}$ when the solution is not depending upon Π_4.

that kp is large enough not to be of much importance in the analysis; therefore, Π_1 will be considered only dependent on Π_2 and Π_3 and the effect of Π_4 will be neglected.

Figure 10B presents the plot of Π_1 as a function of the product $\Pi_2\Pi_3$ for the 1D and 2D problems, for a set of 300 runs for different values of the involved variables, allowing us to collapse the data and fit the curve presented in the figure. Both solutions, 1D and 2D, are exactly the same when the horizontal dimensions are expressed in terms of surface area. Using the suggested values for S_p = 200 g L^{-1} and S_m = 500 g L^{-1}, the fitted curve is valid for $0 \le S_o \le 70$, and is given by

$$\frac{\Omega E_o}{Q_o} = 4.1\left(\frac{S_o}{1250}\right)^{0.76} + 1 \tag{8}$$

with a standard error of 0.005, equivalent to 0.5% for a reference value of $E_o \Omega Q_o^{-1} = 1$.

A second analysis deals with the spatial distribution of salinity. For the sake of simplicity, it is assumed that $\Pi_2 = S_p S_m^{-1}$ is constant with S_p = 200 g L^{-1} and S_m = 500 g L^{-1}, and Π_4 is large enough such that its effect can be neglected, as in the previous analysis. Under these conditions, computed longitudinal salinity profiles, normalized by S_p, are plotted in Fig. 11 in terms of the dimensionless surface area ($\Omega E_o Q_o^{-1}$). Once again 1D and 2D cases yield exactly the same solution, which shows that the spatial distribution of salinity as well as the total area of the VCL are, as a first approximation, independent on the lagoon morphology, and so this analysis and the proposed expression for the dimensionless area of the system can be used in any endorheic lagoon characterized by evapoconcentration.

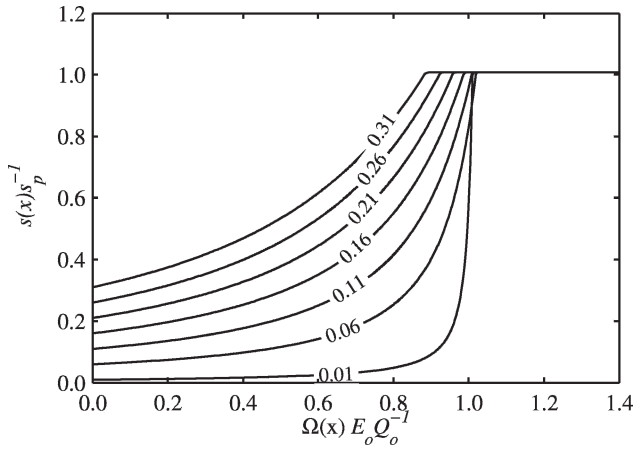

Fig. 11. Longitudinal profiles of normalized salinity as a function of the dimensionless cumulative surface area for different values of inflow salinity S_o normalized by S_p. 1D and 2D approaches yield the same solution. Labels indicate $S_o S_p^{-1}$ values corresponding to each line.

Discussion

Boxlike (i.e., zero-D) approaches have been used to describe salty lagoons and to quantify changes in their ecological features due to changes in external forcing conditions, such as climate changes or modification of hydrological conditions (Evans and Prepas 1996; del Castillo and Farfán 1997; López-González et al. 1998). Timms (2005) described a theoretical model for ecological shifts in Australian salty lagoons due to changes in the salinity and nutrient input, showing that changes in nutrient inputs move the ecosystem between phytoplankton or macrophyte domination, whereas water salinity increases move the ecosystem from macrophyte domination toward microbial mat domination.

In the analyzed VCL system, because of the observed longitudinal salinity gradients, both the macrophyte and microbial mat stages described by Timms (2005) are present simultaneously along it, as described previously, with the former found in the marshland area and the latter in the channel and lagoon areas. The system even shows presence of ichthyofauna in some of the pools in the marshlands area (Parenti 1984). This suggests that the study of small-size aquatic systems such as the VCL should be addressed using conceptual models based on a continuum approach rather than on the traditional boxlike approach, which is somehow embedded in the VCL subdivision too. Taking into account the spatial variability of the system provides a better description of its dynamics. For instance, the presence or absence of macrophytes in the low-salinity areas of the VCLs mostly depends on the inflow water salinity rather than on the inflow water volume or evaporation rates. On the other hand, changes in the inflow volumes will change the total lagoon surface, but the partitioning between salty and fresher-water areas should remain constant.

With respect to the particular analysis of VCL2, extreme meteorological conditions impose high diurnal oscillation of the water temperature in VCL2, between almost 0°C to 30°C in the period of analysis. Among the different fluxes involved in the heat balance, it is concluded that the evaporative heat flux balances the net solar radiation, these two atmospheric fluxes being the most important ones in this balance. However, the heat flux to and from the bottom sediments was identified to be another important factor in the heat balance, contributing to damping the strong oscillations of the water temperature that would occur in case this flux is neglected or not considered.

Furthermore, it was shown that the water temperature appears to be spatially homogeneous, suggesting that heat exchanges with the atmosphere and bottom sediments are also spatially homogeneous. Since heat exchange with bottom sediments is usually controlled by turbulence, this may lead to the idea that the flow conditions or water column turbulence can also be assumed to be spatially homogeneous. However, spatial differences in flow conditions can be clearly seen in the system. This apparent contradiction implies that, although there are spatial differences in the flow conditions, the actual importance of the associated gradients in the system is small with respect to other external agents, such as, for instance, the periodic wind that blows every afternoon with large magnitude. Wind is an external source of energy that affects the entire VCL system, being strong enough to control the water–atmosphere heat fluxes and to impose a Couette-like flow that determines the vertical distribution of shear stress in the water column. This analysis shows that, physically, there are no relevant spatial differences that explain the well-reported spatial biological diversity in VCL2, except for those exhibited by the water salinity. Hence, salinity gradients should be explicitly considered when studying, for instance, the interaction between flamingo populations and benthic organisms in the system (Hulbert and Chang 1983; Demergasso et al. 2003; Herbst 2006).

Regarding the spatial distribution of salinity, the relationship between the inflow volume and the evaporation rate was found to be a function of the inflow salinity S_o. Higher values of S_o decrease the net evaporation rate and increase the surface area of the VCL, decreasing the longitudinal salinity gradients in the system. It was also concluded that the influence of salinity on the evaporation and precipitation rates must be accounted for in any analysis of the VCL systems. Without any of these two processes, the solution of the volume and mass balances would lead to singularities, such as infinite salinity in the case when the relationship between the evaporation rate and salinity is not considered, or infinite surface area of the system in the case when the salt precipitation process is not considered.

Further research should be conducted to, first, validate the coefficients estimated here, and then focus on the temporal changes of water salinity. Regarding the last issue, two aspects present in the meteorological conditions affecting the VCL system studied should impose temporal changes of the spatial distribution of the salinity: daily and subdaily changes in the evaporation rate, which, according to this analysis, varies from 0 up to 40 mm d^{-1} in January, and the wind, which blows periodically from the lagoon to the wetland when it is at maximum magnitude.

Because of the extremely shallow conditions of the VCL systems, processes involved in conservation laws of mass, energy, and volume are primarily driven by air–water

exchanges, which affect the system homogeneously. Coupled interaction among salt evapoconcentration, salt precipitation, and evaporation provides a reasonable explanation for the observed spatial distribution of water salinity.

Acknowledgments

We thank M. Contreras and F. Novoa of Centro de Ecología Aplicada for their support and comments on this manuscript, and to the anonymous reviewers of this article for their useful comments.

A.d.l.F. thanks the fellowship granted by Mejoramiento de la Calidad de la Educación Superior (MECESUP) under project UCH0310. Y.N. thanks the support of Fondecyt Project 1080617.

This article can be also found as a Centre for Water Research Reference number 2280-AF.

References

Adams, E., D. Cosler, and K. Helfrich. 1990. Evaporation from heated water bodies: Predicting combined forced plus free convection. Water Resour. Res. **26:** 425–435.

Benduhn, F., and P. Renard. 2004. A dynamic model of the Aral Sea water and salt balance. J. Mar. Syst. **47:** 35–50.

Birchoff, J., I. Israde-Alcántara, V. Garduño-Monry, and W. Shanks. 2004. The springs of Lake Pátzcuaro: Chemistry, salt-balance, and implications from the water balance of the lake. Appl. Geochem. **19:** 1827–1835.

Bogan, T., O. Mohseni, and H. Stefan. 2003. Stream temperature–equilibrium temperature relationship. Water Resour. Res. **39:** 1245.

Campbell, C. 1995. Temporal salinity variation in salt evaporation basins in south-eastern Australia. Int. J. Salt Lakes Res. **4:** 45–55.

Costelloe, J., E. Irvine, A. Western, and A. Herczeg. 2009. Groundwater recharge and discharge dynamics in an arid-zone ephemeral lake system, Australia. Limnol. Oceanogr. **54:** 86–100.

de la Fuente, A., Y. Niño, and M. Contreras. 2006. A numerical scheme for 2D mass transport and Saint-Venant equations with buoyancy effects. Application to a shallow flow in salt lake Punta Negra, Northern Chile. *In* P. Goubesville, J. Cunge, V. Guinot, and S. Y. Liong [eds.], Proceedings of the 7th International Conference on Hydroinformatics.

del Castillo, E., and C. Farfán. 1997. Hydrobiology of a salt pan from the Peninsula of Baja California, Mexico. Int. J. Salt Lakes Res. **6:** 233–248.

Demergasso, C., G. Chong, P. Galleguillos, L. Escudero, M. Martínez-Alonso, and I. Esteve. 2003. Microbial mats from the Llamará salt flat, nothern Chile. Rev. Chil. Hist. Nat. **76:** 485–499. [In Spanish.]

Evans, J. C., and E. E. Prepas. 1996. Potential effects of climate change on ion chemistry and phytoplankton communities in prairie saline lakes. Limnol. Oceanogr. **41:** 1063–1076.

Garratt, J. R. 1992. The atmospheric boundary layer. Cambridge Univ. Press.

Gulliver, J., and C. Song. 1986. Dynamic roughness and the transition between wind wave regimes. J. Geophys. Res. **91:** 5145–5151.

Helczeg, A., and D. Imboden. 1988. Tritium hydrology studies in four closed-basin lakes in the Great Basin, USA. Limnol. Oceanogr. **33:** 157–173.

Herbst, D. 2006. Salinity controls on trophic interactions among invertebrates and algae of solar evaporation ponds in the Mojave dessert and relation to shorebird foraging and selenium risk. Wetlands **26:** 475–485.

Houston, J. 2007. Recharge to groundwater in the Turi Basin, Northern Chile: An evaluation based on tritium and chloride mass balance techniques. J. Hydrol. **334:** 534–544.

Hulbert, S., and C. Chang. 1983. Ornitholimnology: Effects of grazing by the Andean Flamingo (*Phoenicoparrus andinus*). Proc. Natl. Acad. Sci. USA **80:** 4766–4769.

———, and J. Keith. 1979. Distribution and spatial patterning of flamingos in the Andean Altiplano. Auk **96:** 328–342.

Jerez, V. 2000. Diversity and geographic distribution patterns of coleoteran insects in desert ecology of the Antofagasta region, Chile. Rev. Chil. Hist. Nat. **73:** 485–499.

Kampf, S., S. Tyler, C. Ortiz, J. Muñoz, and P. Adkins. 2005. Evaporation and land surface energy budget at the Salar de Atacama, Northern Chile. J. Hydrol. **310:** 236–252.

Lensky, N., Y. Dvorkin, V. Lyakhovsky, I. Gartmand, and I. Gavrieli. 2005. Water, salt, and energy balances of the Dead Sea. Water Resour. Res. **41:** W12418, doi: 10.1029/2005WR004048.

López-González, P. J., F. Guerrero, and M. C. Castro. 1998. Seasonal fluctuation in the phytoplankton community in a hypersaline temporary lake (Honda, southern Spain). Int. J. Salt Lakes Res. **6:** 353–371.

Mahrt, L., and M. Ek. 1984. The influence of atmospheric stability on potential evaporation. J. Clim. Appl. Meteorol. **23:** 222–234.

Mascitti, V., and F. Kravetz. 2002. Bill morphology of the South American flamingos. Condor **104:** 73–83.

Messerli, B., M. Grosjean, and M. Vuille. 1997. Water availability, protected areas, and natural resources in the Andean desert altiplano. Mt. Res. Dev. **17:** 229–238.

Oround, I. M. 1999. Temperature and evaporation dynamics of saline solution. J. Hydrol. **226:** 1–10.

Parenti, L. R. 1984. A taxonomic revision of the Andean killifish genus *Orestias* (Cyprinodontiformes, Cyprinodontidae). Bull. Am. Mus. Nat. Hist. **178:** 107–214.

Risacher, F., H. Alonso, and C. Salazar. 2003. The origin of brines and salts in Chilean salars: A hydrochemical review. Earth Sci. Rev. **64:** 249–293.

Rosen, M. R. 1994. The importance of groundwater in playas: A review of playa classifications and the sedimentology and hydrology of playas, p. 1–18. *In* M. R. Rosen [ed.], Paleoclimate and basin evolution of playa systems. Geological Society of America. Special Paper.

Rundel, P., A. Gibson, G. Midgley, S. Wand, B. Palma, J. Kleier, and J. Lambrinos. 2003. Ecological and ecophysiological patterns in a pre-altiplano shrubland of the Andean Cordillera in northern Chile. Plant Ecol. **169:** 179–193.

Ryves, D., R. Battarbee, S. Juggins, and N. Anderson. 2006. Physical and chemical predictors of diatoms dissolution in freshwater and saline lake sediments in North America and West Greenland. Limnol. Oceanogr. **51:** 1355–1368.

Timms, B. 2005. Salt lakes in Australia: Present problems and prognosis for the future. Hydrobiologia **552:** 1–15.

Williams, W. 2002. Environmental threats to salt lakes and the likely status of inland saline ecosystems in 2025. Environ. Conserv. **29:** 154–167.

———, T. Carrick, I. Bayly, J. Green, and D. Herbst. 1995. Invertebrates in salt lakes of the Bolivian Altiplano. Int. J. Salt Lakes Res. **4:** 65–77.

Zuñiga, L., V. Campos, H. Pinochet, and B. Prado. 1991. A limnological reconnaissance of Lake Tebenquiche, Salar de Atacama, Chile. Hydrobiologia **210:** 19–24.

Associate editor: H. Maurice Valett

Received: 26 March 2009
Accepted: 09 September 2009
Amended: 29 September 2009